Pollution, 5(4): 879-893, Autumn 2019
DOI: 10.22059/poll.2019.272588.560
Print ISSN: 2383-451X Online ISSN: 2383-4501
Web Page: https://jpoll.ut.ac.ir, Email: jpoll@ut.ac.ir

Evaluation of Catalytic Effects of Metal Oxide Nanoparticles on Pyrolysis of Used Lubricating Oil

Alavi, S. E.[1], Abdoli, M. A.[1*], Khorasheh, F.[2] and Bayandori Moghaddam, A.[3*]

1. School of Environment, College of Engineering, University of Tehran, P.O.Box 14155-6135, Tehran, Iran

2. Department of Chemical and Petroleum Engineering, Sharif University of Technology, Tehran, Iran

3. School of Engineering Science, College of Engineering, University of Tehran, P.O. Box: 11155-4563, Tehran, Iran

Received: 29.11.2018 Accepted: 27.02.2019

ABSTRACT: Pyrolysis is an applicable method that has been widely used to recover hydrocarbons from Used Lubricating Oil (ULO). However, large-scale application of this approach has been limited by its noticeably energy and time consuming nature. In the present research, it has been attempted to modify the energy and time requirements of ULO pyrolysis using the catalytic effects of metal oxide nanoparticles (NPs). The impacts of γ-Al_2O_3, γ-Fe_2O_3 and ZnO NPs on the kinetic features of ULO pyrolysis were studied using thermogravimetric analysis (TGA). The kinetic parameters of the pyrolysis process were calculated based on Kissinger-Akahira-Sunose (KAS) and Flynn-Wall-Ozava (FWO) models. The activation energy of virgin ULO pyrolysis had been calculated to be 161.505 and 162.087 kJ/mol using KAS and FWO models, respectively. However, in the present work, utilization of γ-Fe_2O_3 NPs significantly reduced the activation energy of ULO pyrolysis to 133.511 and 138.289 kJ/mol through KAS and FWO models, respectively. The catalytic effect of ZnO NPs was not as noticeable as that of γ-Fe_2O_3 NPs, resulting in activation energies of 155.568 and 158.501 kJ/mol using KAS and FWO models, respectively. Moreover, based on the results of this study, γ-Al_2O_3 NPs had no significant impact on the kinetics of ULO pyrolysis.

Keywords: Lubricating Oil; Recovery; Kinetic study; Catalytic Effect; Nanoparticle.

INTRODUCTION

Heavy organic compounds are among hardly-decomposable contaminants that can be hazardous for humans, animals and plants when they are discharged into the environment without any treatment (Venegas et al. 2015). Used lubricating oil (ULO) of automobiles, industrial machineries and petroleum refineries is one of the most hazardous compounds which can contaminate soil and water even in very low concentrations due to the presence of various materials such as aromatics and phenols. It can remain in the environment for a long time, due to its negligible biodegradability (Botas et al. 2017; Hassanain et al. 2017). Therefore, discharging untreated ULO into the environment is strictly prohibited by environmental regulations (Kanokkantapong et al. 2009). Besides, ULO treatment can facilitate its recovery and reuse and also promote the process sustainability (Hamad et

* Corresponding Authors, Email: mabdoli@ut.ac.ir & bayandori@ut.ac.ir

al. 2005). Thus in recent years, numerous attempts have been made to find an efficient method for ULO recovery.

Among various influential parameters that can be taken into account when choosing the best recovery method, temperature, operational costs and the quality of ultimate recovered product are considered as the most important ones (Jafari and Hassanpour 2015). Thermal processes such as cracking, hydrotreating and pyrolysis techniques have attracted a great deal of attention, as they result in ultimate products with noticeable qualities and can be applied in large industrial scales (Kim et al. 2013; Manasomboonphan and Junyapoon 2012; Permsubscul et al. 2007; Wang et al. 2016). However, the significantly time and energy consuming nature of these methods will elevate the operational costs and raise doubts about their application in industrial scales (Fuentes et al. 2007).

Therefore, kinetic modification of these methods has become the subject of several researches. Finding an appropriate catalyst that is capable of modifying the kinetic parameters of the recovery process to reduce the required temperature has been the main focus of recent studies (Mortensen et al. 2011). Nanomaterials including nanoparticles and Carbon-based nanostructures, zeolites and biochar are the materials which have drawn the attentions to themselves during last year as the catalysts which can improve the kinetic conditions of pyrolysis process, significantly (Das et al. 2017; Meynet et al. 2014; Rehan et al. 2017).

Metallic NPs have been widely utilized as catalysts in different applications, due to their considerable specific surface area (SSA) and great stability at high temperatures (Gawande et al. 2016; Liu 2006). In this regard, many attempts have been made to improve hydrocarbon recovery and thermal treatment using metallic NPs (Armstrong et al. 2003; Bera and Belhaj 2016). Hosseinpour et al. (2014) have used Co_3O_4, NiO, CuO, Mn_2O_3, Fe_2O_3, and WO_3 nanoparticles to improve the pyrolysis of asphaltene towards advanced in-situ combustion enhanced oil recovery (EOR). According to their findings, NiO and Co_3O_4 had the greatest and lowest adsorption capacities towards asphaltene, respectively. However, according to the calculated activation energies for asphaltene oxidation, WO_3 and Co_3O_4 needed the greatest and lowest levels of activation energy for asphaltene oxidation. In other words, higher redox activities of metal oxides are associated with lower activation energies (Hosseinpour et al. 2014). Amrollahi Biyouki et al. (2017) studied in-situ combustion in the presence of catalytic metal oxide NPs as a method of EOR for heavy oil reservoirs. NiO nanoparticles were dispersed in heavy oil model solutions of asphaltene in toluene-vacuum gasoil. The droplet size, stability and interface elasticity of the emulsions were also monitored. According to the results of their research, the in-situ synthesized NiO nanoparticles increased the coke formation tendency by almost 48% and lowered the coke combustion temperature by about 130 °C. Moreover, the viscosity of the model oil decreased by 2–8% during the in-situ synthesis procedure, indicating an in-situ upgrading potential for the process (Biyouki et al. 2017). Naz et al (2014) applied zeolites to convert ULO to diesel fuel through pyrolysis at 500°C. The chemical composition of the prepared diesel included saturated and unsaturated hydrocarbons with carbon chain in the range of C9-C27. Furthermore, the synthetized diesel showed a noticeable energy recovery (by 85-90%) from ULO and was comparatively impurity-free, with low levels of sulphur, oxygen, and polycyclic aromatic hydrocarbons (PAHs) (Naz et al. 2014).

In this research, the catalytic impacts of metal oxide NPs (γ-Al_2O_3, γ-Fe_2O_3 and ZnO) on ULO pyrolysis studied and their modifications on the kinetic parameters of the process were compared with each

other. Thermogravimetric analysis (TGA) was used to study the differences between ULO samples during the pyrolysis process. Kissinger-Akahira-Sunose (KAS) and Flynn-Wall-Ozava (FWO) models were applied to calculate the kinetic effects of metal oxide NPs on the pyrolysis process.

MATERIAL AND METHODS

The automobile ULO used in this research was collected from a garage in Tehran (Iran) and its specifications have been presented in Table 1.

Thermogravimetric analysis (TGA) was conducted to study ULO pyrolysis. At the first stage, a sample of ULO without any catalyst was analyzed using a TGA METTLER TOLEDO device (TGA/DSC1, Switzerland). The initial weight of the sample in each test was about 10-12 mg. Tests were conducted at heating rates of 5, 10 and 20 °C/min over the temperature range of 25 to 600°C (Liu et al. 2015; Syed et al. 2011). In the next step, the mixtures of ULO and each metal oxide nanoparticle at a concentration of 500 mg/L were prepared and ultra sonicated for 30 minutes at 50°C to prevent NPs agglomeration and provide a homogenous dispersion of NPs in the sample (Taurozzi et al. 2011). All samples were studied using TGA at the same heating rate and temperature range so as to determine the impacts of each metal oxide NP on ULO pyrolysis. Nitrogen gas with flowrate of 50mg/L is used during the pyrolysis process as the inert gas.

γ-Al_2O_3, γ-Fe_2O_3 and ZnO are among the most commonly used nanoparticles in environmental and hydrocarbon recovery applications, due to their high stability at different pressures and temperatures and providing a noticeable SSA (Latiff et al. 2011; Negin et al. 2016; Nezhdbahadori et al. 2018). Metal oxide NPs used in this study were bought from Neutrino® Ltd. (Iran) and their specifications have been shown in Table 2.

Table 1. ULO Specifications

Parameters	Test Results	Parameters	Results
Appearance	Dark	Ultimate Analysis (wt%)	
Density 15 °C (g/cm^3)	0.8854	C	84.21
Specific Gravity (15/4 °C)	0.8861	H	13.43
API Gravity	28.2	N	ND
Viscosity 40°C (cSt)	102.3	S	0.54
Viscosity 100°C (cSt)	11.2	Metals Content (ppm)	
Flash Point (°C)	174	Ba	<5
		Al	<5
Proximate analysis (wt%)		Cr	<5
Volatile Matters	97.7	Cu	<5
Ashes	1.3	Zn	721
Moisture	0.85	Fe	68
		Ni	<5

Table 2. metal oxide NPs specifications

Formula	Al_2O_3	Fe_2O_3	ZnO
Phase	Gamma	Gamma	-
Purity	99.9%	99%	99.9%
Average Particle size	20 nm	25 nm	45 nm
SSA	120 m^2/g	50 m^2/g	40 m^2/g
Morphology	Spherical	Spherical	Spherical
Density	3.65 g/cm^3	5.24 g/cm^3	5.6 g/cm^3
Appearance	White powder	Red brown powder	White
Molecular weight	101.96 g/mol	159.69 g/mol	81.37 g/mol

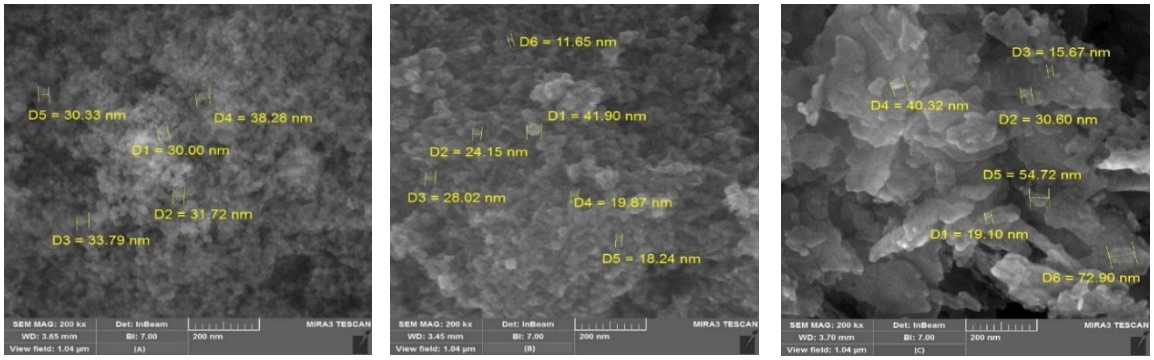

Fig. 1. SEM images for (A) γ-Al_2O_3, (B) γ-Fe_2O_3 and (C) ZnO nanoparticles

Scanning electron microscopy (SEM) using MIRA3 instrument (TESCAN, US) was conducted to characterize the nanoparticles used in this study (γ-Al_2O_3, γ-Fe_2O_3, and ZnO). During the tests, SEM magnification was 200 kX with a 200 nm scale for each metal oxide NPs sample. Figure 1 shows the SEM images of metal oxide NPs used in this study.

As it can be seen in the figure, the sizes of γ-Al2O3, γ-Fe2O3 and ZnO NPs were in the ranges of 30 to 38 nm, 11 to 42 nm and 15 to 73 nm, respectively.

TGA has been frequently used to calculate the kinetic parameters of hydrocarbon compound decomposition during pyrolysis (Barneto et al. 2014; Kim et al. 2003). Kissinger-Akahira-Sunose (KAS) and Flynn-Wall-Ozava (FWO) methods are two commonly used models for kinetic analysis of pyrolysis process, due to their generality, desirable accuracy and rational assumptions (Flynn and Wall 1966; Kissinger 1957; Vyazovkin 2008).

Kinetic study using TGA is based on variations of sample weight with time and temperature. In all TGA tests, the degree of conversion (X) plays the key role in the calculation of kinetic parameters. It can be obtained using Eq. 1:

$$X = \frac{w}{w_0 - w_\infty} \quad (1)$$

Here, w_0, w and w_∞ denote the initial weight and the weights of paralyzed and unpyrolyzed fractions of the sample, respectively (Kim et al. 2013).

Kinetic calculations in both KAS and FWO models are started with the equation of reaction rate. The rate of reaction (dX/dt) in a thermal transformation can be written as Eq. 2 (Coats and Redfern 1964):

$$\frac{dX}{dt} = \beta \frac{dX}{dT} = K(T) f(X) \quad (2) \qquad (2)$$

where K(T) and f(X) are functions of temperature and conversion, respectively, and β is the heating rate during the process.

As it has been shown in Eq. 2, K (T) is dependent on the temperature. It can be defined through Arrhenius equation, as below (Vyazovkin 2008):

$$K(T) = k_0 \exp\left(\frac{-E_0}{RT}\right) \quad (3)$$

k_0 is Arrhenius coefficient, which is normally known as frequency factor. E_0, R and T in Eq. 3 are activation energy, the universal gas constant and absolute temperature, respectively. One can rewrite Eq. 2 based on Eq. 3, to obtain the following expression:

$$\frac{dX}{f(x)} = \frac{k_0}{\beta} \exp\left(\frac{-E_0}{RT}\right) dT \quad (4)$$

Integration of Eq. 4 under the initial conditions of X=0 at $T=T_0$ (here, 25°C) results in Eq. 5 which is the general kinetic equation of the reaction based on temperature and kinetic parameters (Aboulkas and El Harfi 2008).

$$g(X)=\int_0^X \frac{dX}{f(X)}=\frac{k_0}{\beta}\int_{T_0}^{T}\exp\left(\frac{-E_0}{RT}\right)dT = \frac{k_0E_0}{\beta R}\,p\left(\frac{E_0}{RT}\right) \quad (5)$$

KAS model is based on the Coats-Redfern approximation which results in the following expression (Coats and Redfern 1964):

$$\ln\frac{\beta}{T^2}=\ln\frac{k_0R}{E_0.g(X)}-\frac{E_0}{RT} \quad (6)$$

On the other hand, FWO method is derived from integration and Doyle's approximation, leading to: $\ln p\left(\frac{E_0}{RT}\right) \cong$-5.331-1.052 $\left(\frac{E_0}{RT}\right)$ (Doyle 1961). Hence, we have:

$$\ln\beta=ln\frac{k_0E_0}{R.g(X)}-5.331-1.052\left(\frac{E_0}{RT}\right) \quad (7)$$

Assuming a first-order reaction, g(X) can be rewritten as Eq. 8 (Vyazovkin et al. 2011):

$$g(X)= -\ln(1-X) \quad (8)$$

Linear fitting of $\ln(\frac{\beta}{T^2})$ and $\ln\beta$ vs $\frac{1}{T}$ data in KAS and FWO methods, respectively, for a constant X (iso-conversional points) at three different heating rates of 5, 10 and 20°C/min, gives line slopes of $\left(-\frac{E_0}{R}\right)$ and $\left(-\frac{1.052\,E_0}{R}\right)$, respectively (Vyazovkin et al. 2011).

RESULTS AND DISCUSSION

In order to study the catalytic effects of metal oxide NPs on the pyrolysis of ULO, it is necessary to first calculate the kinetic parameters (i.e. activation energy and frequency factor) of virgin ULO. In our previous in-detail kinetic study on the virgin ULO, the average activation energy of virgin ULO using KAS and FWO models was calculated to be 161.505 and 162.087 kJ/mol, respectively.

TGA was performed to determine the kinetic parameters of the pyrolysis process after applying metal oxide NPs. The results are shown in Figures 2 and 3.

As shown in Figure 2, application of γ-Fe_2O_3 NPs has significantly changed the variations of X with temperature. The presence of γ-Fe_2O_3 NPs resulted in a relative maximum (around 100°C) in the TGA graph of ULO. Based on the data shown in Table 1 (indicating a negligible moisture level in the ULO sample), it can be concluded that the sudden increase in the conversion slope must be due to the considerable affinity of highly volatile components towards γ-Fe_2O_3 NPs and their catalytic effects in the reaction. This trend was also observable in Figure 3, where the highest rate of reaction occured at around 100°C with a very high slope, followed by a sudden drop. Thereafter, the rate of reaction for the case of ULO+ γ-Fe_2O_3 NPs increased with approximately the same slope as virgin ULO, until it plateaued at the maximum X level.

Compared to γ-Fe_2O_3 NPs, a similar phenomena with a lesser effect could be observed for ZnO NPs. Application of these NPs generated a relative maximum point in the TGA graph, which was probably due to the adsorption of highly volatile components and the catalytic impacts of NPs. However, the effects of such factors in both TGA and DTG graphs were less than those for the peak of γ-Fe_2O_3 NPs, because of the lower affinity of ZnO towards volatile hydrocarbons (Ghaffari et al. 2017).

γ-Al_2O_3 NPs did not make any significant change in ULO pyrolysis, despite their high SSA and incapability of breaking carbon bonds among hydrocarbon molecules.

According to Figures 2 and 3, the presence of γ-Fe_2O_3 NPs not only decreased the temperature of maximum conversion for ULO, but also reduced the temperature at which the maximum rate of pyrolysis is achieved. Since the sample is continously heated during TGA, it is predicted that the time of decomposition

decreases when γ-Fe_2O_3 NPs are present in the sample.

Since TGA results were indicative of negligible impacts of γ-Al_2O_3 NPs on ULO pyrolysis, further kinetic studies were only performed in the case of γ-Fe_2O_3 and ZnO using KAS and FWO models.

Figure 4 shows the TGA results for ULO pyrolysis in the prsence of γ-Fe_2O_3 NPs at three different heating rates.

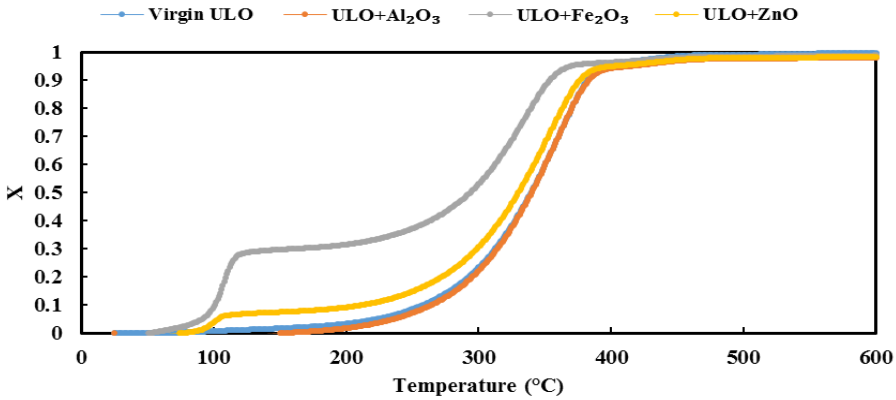

Fig. 2. TGA curves for ULO pyrolysis in the presence and absence of MNPs, at the heating rate of 20 °C/min

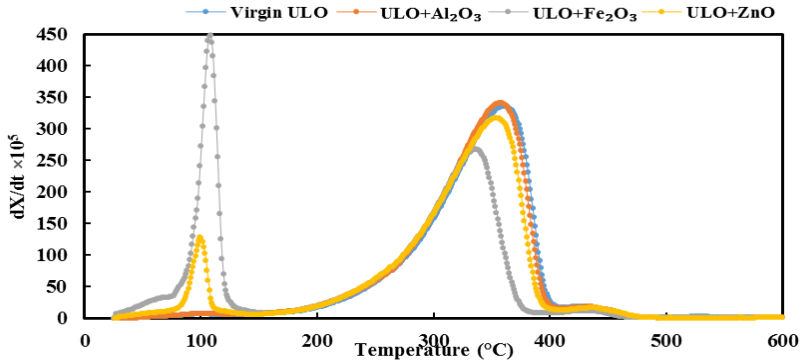

Fig. 3. DTG curves for ULO pyrolysis in the presence and absence of nanomaterials, at the heating rate of 20 °C/min

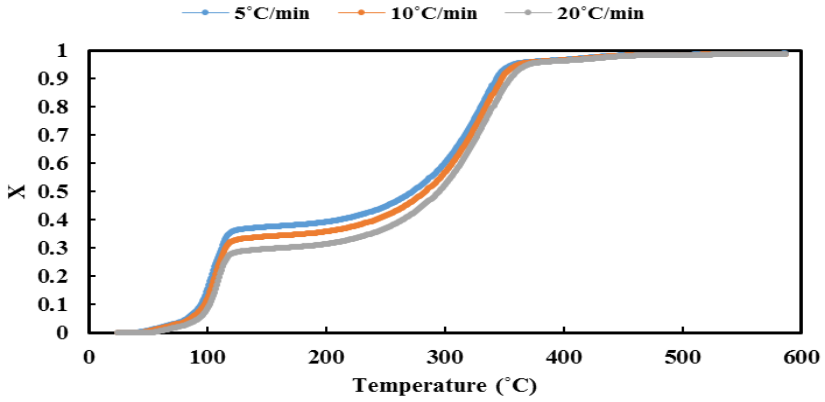

Fig. 4. TGA results for ULO pyrolysis in the presence of γ-Fe_2O_3 NPs at three heating rates of 5, 10 and 20 °C/min.

As depicted in Figure 4, there was a sharp increase in X in the range of 80 to 120˚C, which was predictable based on Figures 2 and 3. This increase was mainly due to the significant affinity of γ-Fe_2O_3 NPs towards highly volatile components. Increasing the heating rate shifted the sharp growth zone to higher temperatures, though the maximum X level (up to which the process could continue with an intensive slope) decreased.

Besides, when the degree of conversion reached its maximum level, the intensity of variation with temperature decreased and the corresponding graph was almost a horizontal line.

The temperature at which the process reached the maximum conversion level was variable, depending on the heating rate. According to Figure 4, as the heating rate increased, the process reached the maximum conversion after a longer time duration, in comparison with lower heating rates.

According to Figure 2 and 4, it can also be concluded that in the presence of γ-Fe_2O_3 NPs, decomposition mainly occures in the temerature range of 100 to 380 ˚C, which is considerably lower than that for virgin ULO (230 to 400˚C).

Figure 5 depictes the differential thermogravimetric graph (DTG) of ULO+ γ-Fe_2O_3 NPs, which was used as the basis of pyrolysis kinetic studies.

As shown in Figure 5, the temperatures at which maximum X occured at different heating rates were very close. Besides, the maximum rate of conversion in pyrolysis was directly dependent on the heating rate. As the heating rate increased, the maximum rate of conversion was also increased.

As explained in the Materials and methods section, in order to calculate the kinetic parameters, it is necessarry to perform linear fitting according to Eqs. 2 to 6. Figure 6 shows the graph of ln $(\frac{\beta}{T^2})$ vs $\frac{1}{T}$ for ten different conversions at three heating rates of 5, 10 and 20°C/min, which gives the kinetic parameters of pyrolysis through KAS model.

Table 3 shows the kinetic parameters of ULO pyrolysis in the presence of γ-Fe_2O_3 NPs which were obtained based on the slopes and intercepts of the fitted lines in Figure 6.

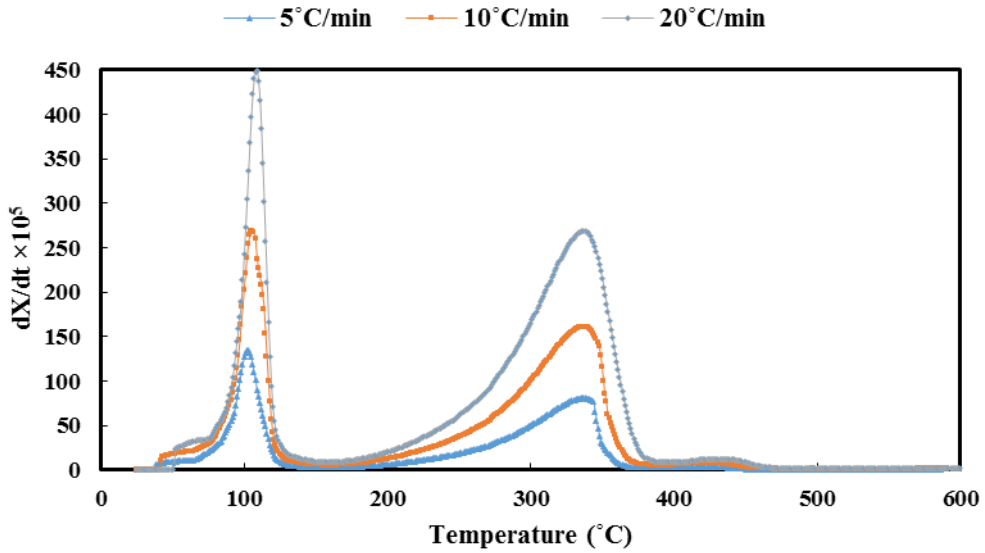

Fig. 5. Changes in the rate of conversion (dX/dt) vs. temperature at heating rates of 5, 10 and 20 °C/min for the pyrolysis of ULO+ γ-Fe_2O_3 NPs

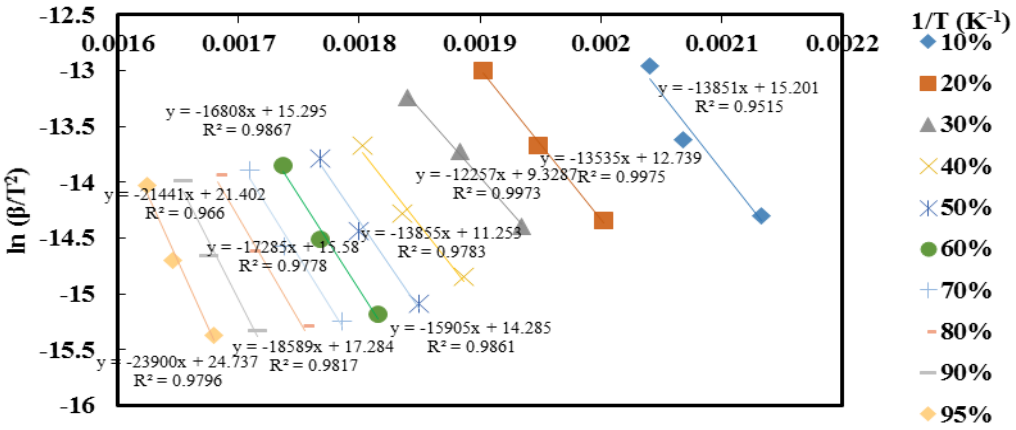

Fig. 6. ln (β/T^2) vs 1/T data for ULO+ γ-Fe_2O_3 NPs at different degrees of conversions (X) and heating rates of 5, 10, 20 °C/min for calculation of pyrolysis kinetic parameters using KAS model.

Table 3. Kinetic parameters of the pyrolysis of ULO+ γ-Fe_2O_3 NPs using the KAS method

X (%)	Activation Energy (kJ/mol)	Arrhenius Constant	R^2
10	115.156	5.5E+10	0.9515
20	112.53	4.6E+09	0.9975
30	101.901	1.4E+08	0.9973
40	115.188	1.1E+09	0.9783
50	132.236	2.5E+10	0.9861
60	139.740	7.4E+10	0.9867
70	143.705	1E+11	0.9778
80	154.545	6E+11	0.9817
90	178.262	4.2E+13	0.9660
95	198.706	1.3E+15	0.9796

According to Figure 6, the average activation energy for pyrolysis of ULO in the presence of γ-Fe_2O_3 NPs was 133.511 kJ/mol. In other words, γ-Fe_2O_3 NPs significantly decreased the activation energy of ULO pyrolysis and consequently increased the process rate.

FWO is another model that can be used to calculate the kinetic parameters of ULO pyrolysis. Figure 7 illustrates the variations of $\ln \beta$ vs. 1/T, which gives the kinetic parameters of pyrolysis in FWO model.

Similar to KAS model, in the case of FWO model, the activation energ and frequency factor for ULO+ γ-Fe_2O_3 NPs pyrolysis were also calculated from the slopes and intrcepts of the fitted lines, as indicated in Table 4.

Based on the data shown in Figure 7, the average activation energy was 138.289 kJ, being approximately equal to the activaton energy calculated from KAS model. This means that regardless of the kinetic model, γ-Fe_2O_3 NPs noticeably decreased the activation energy of ULO pyrolysis, which is the most important evidence for their catalytic effect.

Similar to the case of γ-Fe_2O_3 NPs, TGA and DTG graphs for ZnO NPs were first obtained for subsequent kinetic studies. Figures 8 and 9 show the TGA and DTG graphs for ULO+ZnO NPs pyrolysis, respectively.

Similar to Figures 4 and 5, the temperature dependencies of maximum X and maximum rate of conversion are obvious in Figures 8 and 9.

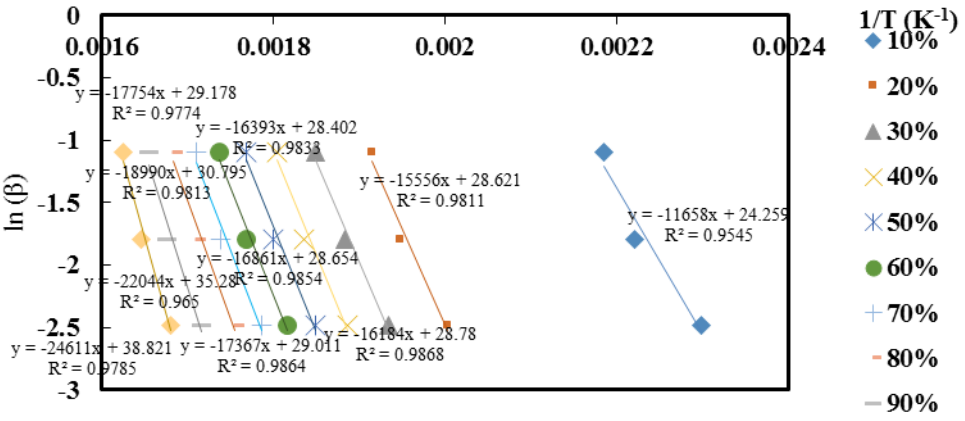

Fig. 7. ln (β) vs. 1/T data for ULO+ γ-Fe_2O_3 NPs at different degrees of conversion (X) and heating rates of 5, 10, 20 °C/min for calculation of pyrolysis kinetic parameters using FWO model

Table 4. Kinetic parameters of the pyrolysis of ULO+ γ-Fe_2O_3 NPs using FWO method

X (%)	Activation Energy (kJ/mol)	Arrhenius Constant	R^2
10	112.860	2.2E+09	0.9545
20	122.936	8.4E+09	0.9811
30	127.904	1.5E+10	0.9868
40	129.557	1.5E+10	0.9833
50	133.250	2.5E+10	0.9854
60	137.253	4.6E+10	0.9864
70	140.312	6.9E+10	0.9774
80	150.081	4.4E+11	0.9813
90	174.213	4.8E+13	0.9650
95	194.504	1.9E+15	0.9785

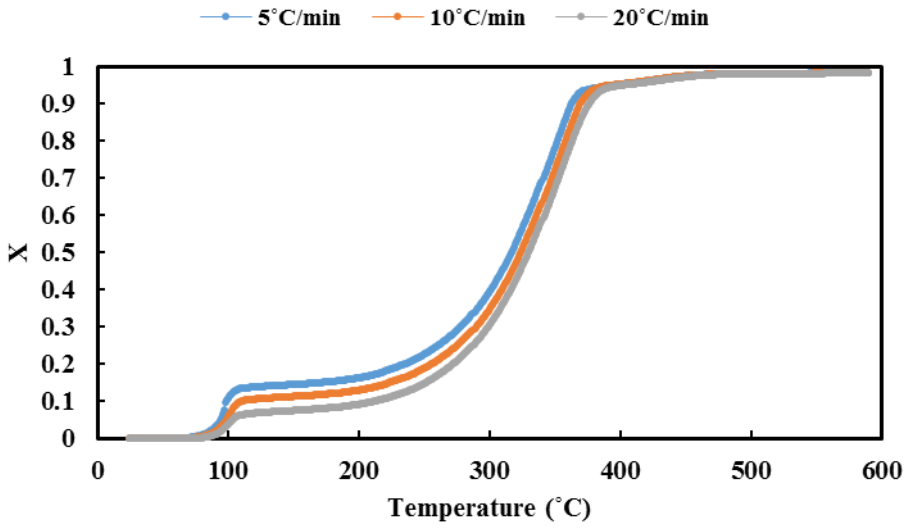

Fig. 8. TGA results for the pyrolysis of ULO+ZnO NPs at three heating rates of 5, 10 and 20 °C/min

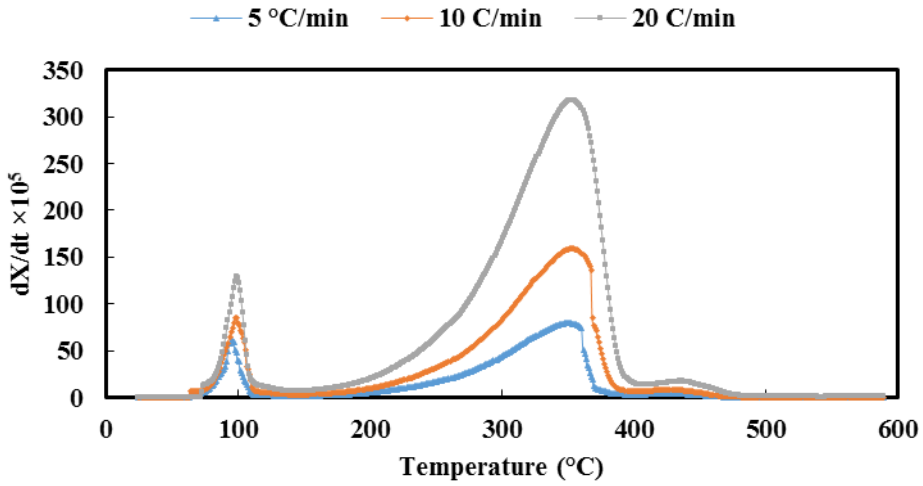

Fig. 9. Changes in the rate of conversion (dX/dt) vs. temperature at heating rates of 5, 10 and 20 °C/min for the pyrolysis of ULO+ZnO NPs

Figure 10 shows the graph of ln ($\frac{\beta}{T^2}$) vs. $\frac{1}{T}$ for ten different conversions at three heating rates of 5, 10 and 20°C/min for the pyrolysis of ULO+ZnO NPs using KAS model.

Based on Figure 10, in this case, the average activation energy was 155.568 kJ/mol. According to Figure 3, it was predicted that ZnO NPs can increase the reaction rate in comparison with the virgin ULO, but their impact would not be as strong as γ-Fe_2O_3 NPs. The results of kinetic study confirmed the accurateley of our prediction.

Similar to the case of γ-Fe_2O_3 NPs, here we applied FWO model to validate the results of kinetic analysis. Figure 11 shows ln β vs. $\frac{1}{T}$ data for ULO+ZnO NPs, which are the basis of kinetic calculations in FWO model.

Table 6 shows the kinetic parameters obtained from Figure 11.

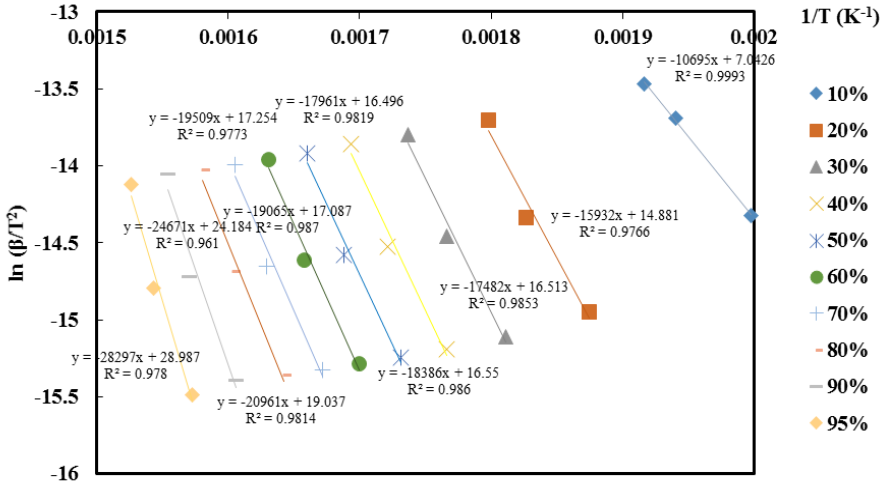

Fig. 10. ln (β/T^2) vs. 1/T data for ULO+ZnO NPs at different degrees of conversion (X) and heating rates of 5, 10, 20 °C/min for calculation of pyrolysis kinetic parameters using KAS model

Table 5. Kinetic parameters of the pyrolysis of ULO+ ZnO NPs using KAS method

X (%)	Activation Energy (kJ/mol)	Arrhenius Constant	R^2
10	88.921	1.2E+07	0.9993
20	132.455	4.6E+10	0.9766
30	145.347	2.6E+11	0.9853
40	149.330	2.6E+11	0.9819
50	152.858	2.8E+11	0.9860
60	158.506	5E+11	0.9870
70	162.196	6.1E+11	0.9773
80	174.271	3.9E+12	0.9814
90	205.113	7.9E+14	0.9610
95	235.265	1.1E+17	0.9780

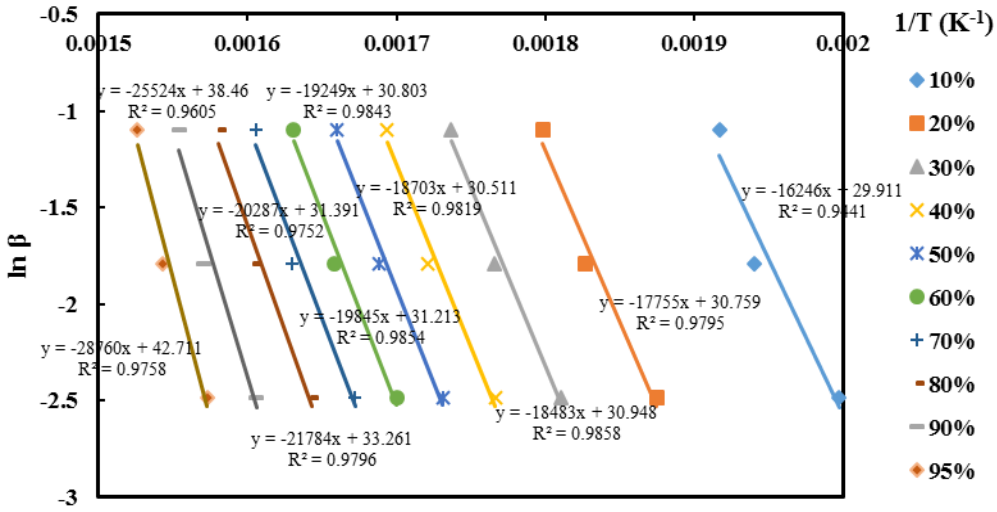

Fig. 11. ln (β) vs. 1/T data for ULO+ZnO NPs at different degrees of conversion (X) and heating rates of 5, 10, 20 °C/min for calculation of pyrolysis kinetic parameters using FWO model

Table 6. Kinetic parameters of the pyrolysis of ULO+ ZnO NPs using FWO method

X (%)	Activation Energy (kJ/mol)	Arrhenius Constant	R^2
10	128.395	1.38E+10	0.9441
20	140.318	6.23E+10	0.9795
30	146.075	1.16E+11	0.9858
40	147.814	1.06E+11	0.9819
50	152.127	1.87E+11	0.9843
60	156.834	3.61E+11	0.9854
70	160.328	5.54E+11	0.9752
80	172.162	4.48E+12	0.9796
90	201.720	9.9E+14	0.9605
95	227.290	8.02E+16	0.9758

The average activation energy for pyrolysis of ULO+ZnO NPs was calculated to be 158.501 kJ/mol using FWO model, which was close to the results of KAS method, indicating the validity of calculations. Figures 12 and 13 show the variations of activation energy vs. X in the ULO sample in the presence of γ-Fe_2O_3 and ZnO NPs using KAS and FWO models, respectively.

As illustrated in Figure 12 and 13, the results of KAS and FWO methods for activation energy calculation were not significantly different, indicating that the kinetic study was valid and the results were reliable.

Besides, according to Figures 12 and 13, the activation energy of pyrolysis increased with the increase in the degree of conversion. A higher degree of conversion is indicative of heavier components which require higher levels of energy for evaporation/cracking. Therefore, it is rational to expect that activation energy slightly increases with the increase in the degree of conversion.

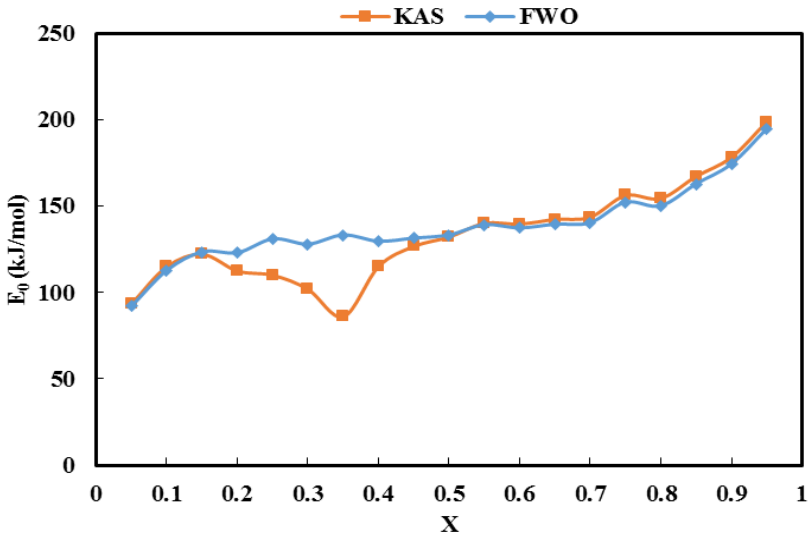

Fig. 12. Activation energy vs degree of conversion in KAS and FWO models for ULO+ γ-Fe_2O_3

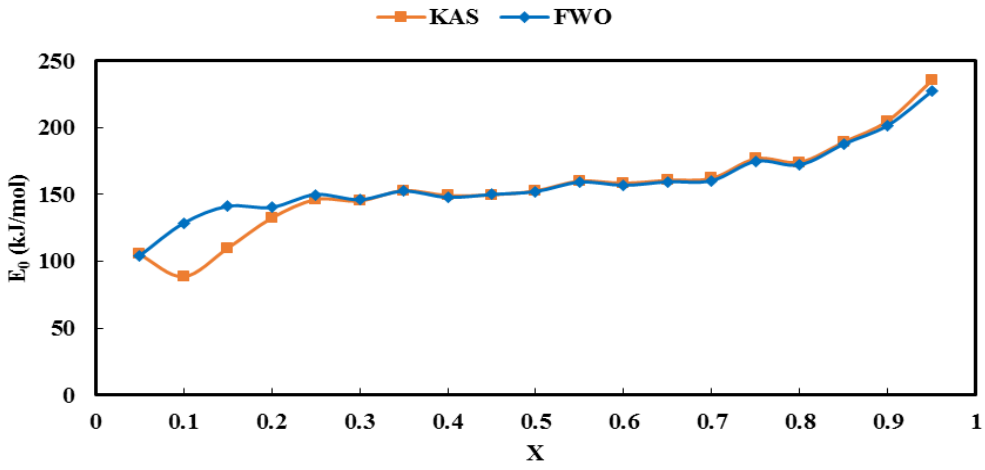

Fig. 13. Activation energy vs degree of conversion in KAS and FWO models for ULO+ZnO

The relations between E_0 and k_0 are in the form of Eqs. 9 to 12 based on FWO and KAS methods for ULO in the presence of γ-Fe_2O_3 and ZnO NPs, respectively (see Figure 14).

$$\ln k_{0,ZnO_{KAS}} = 0.1411E_0 + 5.1904 \, , R^2 = 0.9667 \quad (9)$$

$$\ln k_{0,ZnO_{FWO}} = 0.1590E_0 + 2.1897 \, , R^2 = 0.9879 \quad (10)$$

$$\ln k_{0,Fe_2O_{3KAS}} = 0.1497E_0 + 4.6034 \, , R^2 = 0.9097 \quad (11)$$

$$\ln k_{0,Fe_2O_{3FWO}} = 0.1695E_0 + 1.7235 \, , R^2 = 0.9888 \quad (12)$$

According to Figure 14 and Eqs. 9 to 12, it can be concluded that the correlation between kinetic parameters using FWO model is more accurate than those determined through KAS model.

It can be concluded from the results that the catalytic strength of the nanoparticles used in this study is as follows:

γ-Fe_2O_3> ZnO> γ-Al_2O_3

which is deductable from the impact they have on activation energy.

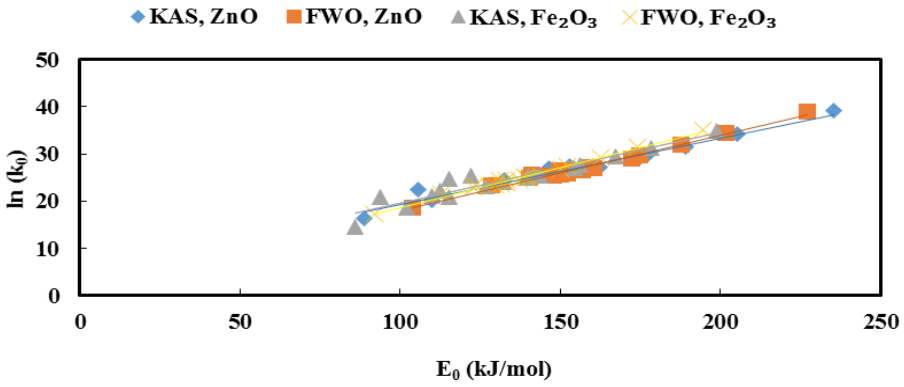

Fig. 14. ln (k_0) vs E_0 in ULO pyrolysis in the presence of γ-Fe_2O_3 and ZnO NPs using KAS and FWO models

According to Fig. 2, γ -iron oxide nanoparicles make a noticeable change in the hydrcarbons conversion in the thermal range of <100˚C which can be mainly due to the high affinity of γ-Fe_2O_3 nanoparticles for absorption of highly-volatile hydrocarbons. γ -iron oxide nanoparticles usually show a core-shell structure with elemental Fe in the core and iron ions in the shell. A combination of electron donation from the core and absorption by the shell is the mechanism which significantly enhances the catalytic strength of iron NPs (Guerra et al. 2018; Raychoudhury and Scheytt 2013).

CONCLUSION

The presence of a wide range of hazardous hydrocarbons in used lubricating oil (ULO) and its high viscosity make it a dangerous pollutant which needs to be treated before being discharged into the environment. The high content of hydrocarbons in this substance has motivated researchers to find an efficient method for their recovery from ULO, which not only neutralizes the harms of this pollutant, but also can significantly make the process more economic. In recent years, the pyrolysis process has attracted a great deal of scientific attention. However, its highly energy and time consuming nature has made it impossible to use pyrolysis in large industrial scales. Utilization of materials with catalytic capabilities can significantly help to improve the kinetics of this process. Metal oxide NPs such as γ-Al_2O_3, γ-Fe_2O_3 and ZnO are among the most applicable catalysts which have been widely utilized in environmental applications in recent years, especially for hydrocarbon recovery. In this research, the catalytic

effects of these three nanoparticles were studied and it was concluded that γ-Fe_2O_3 NPs can significantly decrease the activation energy of the pyrolysis process and kinetically improve the whole process. Though the effects of ZnO NPs were not as intensive as Fe_2O_3, but their performance was better than γ-Al_2O_3 NPs which showed no noticeable catalytic activity towards ULO pyrolysis. The results of this research can be a very good basis for further studies on catalytic effects of other metallic nanoparticles or a specific combination of such materials for hydrocarbon recovery from different oily wastes.

REFERENCES

Aboulkas, A. and El Harfi, K. (2008). Study of the Kinetics and Mechanisms of Thermal Decomposition of Moroccan Tarfaya Oil Shale and Its Kerogen. Oil Shale 25(4).

Armstrong, R., Baschung, B., Booth, D. and Samirant, M. (2003). Enhanced propellant combustion with nanoparticles. Nano Letters 3(2):253-255.

Barneto, A.G., Moltó, J., Ariza, J. and Conesa, J.A. (2014). Thermogravimetric monitoring of oil refinery sludge. Journal of Analytical and Applied Pyrolysis 105:8-13.

Bera, A. and Belhaj, H. (2016). Application of nanotechnology by means of nanoparticles and nanodispersions in oil recovery-A comprehensive review. Journal of Natural Gas Science and Engineering 34:1284-1309.

Biyouki, A.A., Hosseinpour, N., Bahramian, A. and Vatani, A. (2017). In-situ upgrading of reservoir oils by in-situ preparation of NiO nanoparticles in thermal enhanced oil recovery processes. Colloids and Surfaces A: Physicochemical and Engineering Aspects 520:289-300.

Botas, J.A., Moreno, J., Espada, J.J., Serrano, D.P. and Dufour, J. (2017). Recycling of used lubricating oil: Evaluation of environmental and energy performance by LCA. Resources, Conservation and Recycling 125:315-323.

Coats, A.W. and Redfern, J. (1964). Kinetic parameters from thermogravimetric data. Nature 201(4914):68.

Das, V.K., Shifrina, Z.B. and Bronstein, L.M. (2017). Graphene and graphene-like materials in biomass conversion: paving the way to the future. Journal of Materials Chemistry A 5(48):25131-25143.

Doyle, C.D. (1961). Kinetic analysis of thermogravimetric data. Journal of applied polymer science 5(15):285-292.

Flynn, J.H. and Wall, L.A. (1966). General treatment of the thermogravimetry of polymers. J Res Nat Bur Stand 70(6):487-523.

Fuentes, M., Font, R., Gómez-Rico, M. and Martín-Gullón, I. (2007). Pyrolysis and combustion of waste lubricant oil from diesel cars: Decomposition and pollutants. Journal of Analytical and Applied Pyrolysis 79(1-2):215-226.

Gawande, M.B., Goswami, A., Felpin, F.X., Asefa, T., Huang, X., Silva, R., Zou, X., Zboril, R. and Varma, R.S. (2016). Cu and Cu-based nanoparticles: synthesis and applications in catalysis. Chemical reviews 116(6):3722-3811.

Ghaffari, S.B, Sarrafzadeh, M.H, Fakhroueian, Z., Shahriari, S. and Khorramizadeh, M.R. (2017). Functionalization of ZnO nanoparticles by 3-mercaptopropionic acid for aqueous curcumin delivery: Synthesis, characterization, and anticancer assessment. Materials Science and Engineering: C 79:465-472.

Guerra, F., Attia, M., Whitehead, D. and Alexis, F. (2018). Nanotechnology for environmental remediation: materials and applications. Molecules 23(7):1760.

Hamad, A., Al-Zubaidy, E. and Fayed, M.E. (2005). Used lubricating oil recycling using hydrocarbon solvents. Journal of environmental management 74(2):153-159.

Hassanain, E.M., Yacout, D.M., Metwally, M. and Hassouna, M. (2017). Life cycle assessment of waste strategies for used lubricating oil. The International Journal of Life Cycle Assessment 22(8):1232-1240.

Hosseinpour, N., Mortazavi, Y., Bahramian, A., Khodatars, L. and Khodadadi, A.A. (2014). Enhanced pyrolysis and oxidation of asphaltenes adsorbed onto transition metal oxides nanoparticles towards advanced in-situ combustion EOR processes by nanotechnology. Applied Catalysis A: General 477:159-171.

Jafari, A.J. and Hassanpour, M. (2015). Analysis and comparison of used lubricants, regenerative technologies in the world. Resources, Conservation and Recycling 103:179-191.

Kanokkantapong, V., Kiatkittipong, W., Panyapinyopol, B., Wongsuchoto, P. and Pavasant, P. (2009). Used lubricating oil management options based on life cycle thinking. Resources, Conservation and Recycling 53(5):294-299.

Kim, S.S., Chun, B.H. and Kim, S.H. (2003). Non-

isothermal pyrolysis of waste automobile lubricating oil in a stirred batch reactor. Chemical Engineering Journal 93(3):225-231.

Kim, S.S., Kim, J., Jeon, J.K., Park, Y.K. and Park, C.J. (2013). Non-isothermal pyrolysis of the mixtures of waste automobile lubricating oil and polystyrene in a stirred batch reactor. Renewable energy 54:241-247.

Kissinger, H.E. (1957). Reaction kinetics in differential thermal analysis. Analytical chemistry 29(11):1702-1706.

Latiff, N.R.A., Yahya, N., Zaid, H.M. and Demiral, B. (2011) Novel enhanced oil recovery method using dielectric zinc oxide nanoparticles activated by electromagnetic waves; IEEE. p 1-7.

Liu, G., Song, H. and Wu, J. (2015). Thermogravimetric study and kinetic analysis of dried industrial sludge pyrolysis. Waste management 41:128-133.

Liu, W.T. (2006). Nanoparticles and their biological and environmental applications. Journal of Bioscience and bioengineering 102(1):1-7.

Manasomboonphan, W. and Junyapoon, S. (2012) Production of liquid fuels from waste lube oils used by pyrolysis process; 2nd International Conference on Biomedical Engineering and Technology. p 130-133.

Meynet, P., Moliterni, E., Davenport, R.J., Sloan, W.T., Camacho, J.V. and Werner, D. (2014). Predicting the effects of biochar on volatile petroleum hydrocarbon biodegradation and emanation from soil: a bacterial community finger-print analysis inferred modelling approach. Soil Biology and Biochemistry 68:20-30.

Mortensen, P.M., Grunwaldt, J.D., Jensen, P.A., Knudsen, K. and Jensen, A.D. (2011). A review of catalytic upgrading of bio-oil to engine fuels. Applied Catalysis A: General 407(1-2):1-19.

Naz, A., Ullah, M., Ali, S.D., Mahmood, T., Siddiq, M., Bano, A. and Tariq, Z. 2014. Nano Catalytic Conversion of used Lubricating Oil into Diesel Fuel. International Journal of Enhanced Research in Science Technology & Engineering 3(4):438-446.

Negin, C., Ali, S. and Xie, Q. (2016). Application of nanotechnology for enhancing oil recovery–A review. Petroleum 2(4):324-333.

Nezhdbahadori, F., Abdoli, M.A, Baghdadi, M. and Ghazban, F. (2018). A comparative study on the efficiency of polar and non-polar solvents in oil sludge recovery using solvent extraction. Environmental monitoring and assessment 190(7):389.

Permsubscul, A., Vitidsant, T. and Damronglerd, S. (2007). Catalytic cracking reaction of used lubricating oil to liquid fuels catalyzed by sulfated zirconia. Korean Journal of Chemical Engineering 24(1):37-43.

Raychoudhury, T. and Scheytt, T. (2013). Potential of zerovalent iron nanoparticles for remediation of environmental organic contaminants in water: a review. Water Science and Technology 68(7):1425-1439.

Rehan, M., Miandad, R., Barakat, M., Ismail, I., Almeelbi, T., Gardy, J., Hassanpour, A., Khan, M., Demirbas, A. and Nizami, A. (2017). Effect of zeolite catalysts on pyrolysis liquid oil. International Biodeterioration & Biodegradation 119:162-175.

Syed, S., Qudaih, R., Talab, I. and Janajreh, I. (2011). Kinetics of pyrolysis and combustion of oil shale sample from thermogravimetric data. Fuel 90(4):1631-1637.

Taurozzi, J.S., Hackley, V.A. and Wiesner, M.R. (2011). Ultrasonic dispersion of nanoparticles for environmental, health and safety assessment–issues and recommendations. Nanotoxicology 5(4):711-729.

Venegas, A., Rigol, A. and Vidal, M. (2015). Viability of organic wastes and biochars as amendments for the remediation of heavy metal-contaminated soils. Chemosphere 119:190-198.

Vyazovkin, S. (2008). The handbook of thermal analysis & calorimetry. Recent Advances, Techniques and Applications 5:503.

Vyazovkin, S., Burnham, A.K., Criado, J.M., Pérez-Maqueda, L.A, Popescu, C. and Sbirrazzuoli, N. (2011). ICTAC Kinetics Committee recommendations for performing kinetic computations on thermal analysis data. Thermochimica acta 520(1-2):1-19.

Wang, F., Li, M.L., Duan, P.G., Fu, J., Lü, X.Y. and Xu, Y.P. (2016). Co-hydrotreating of used engine oil and the low-boiling fraction of bio-oil blends for the production of liquid fuel. Fuel Processing Technology 146:62-69.